TRAJECTORIES OF MESOSCALE EDDIES IN THE NORTHWESTERN REGION OF THE HAWAIIAN ISLANDS DERIVED FROM SEA SURFACE HEIGHT ALTIMETRY DATA

A SENIOR THESIS SUBMITTED TO THE GLOBAL ENVIRONMENTAL SCIENCES UNDERGRAUATE DIVISION OF THE UNIVERSITY OF HAWAII AT MANOA IN PARTIAL FULFILMENT OF THE REQUIREMENT FOR THE DEGREE OF

BACHELOR OF SCIENCE

IN

GLOBAL ENVIRONMENTAL SCIENCE

DECEMBER 2004

By

Kazuhiro Nakagawa

Thesis Advisor:

Bo Qiu

I certify that I have read this thesis and that, in my opinion, it is satisfactory in scope and quality as a thesis for the degree of Bachelor of Science in Global Environmental Science.

THESIS ADVISOR

Bo Qiu
Department of Oceanography

ACKNOWLEDGEMENT

I would like to thank my thesis advisor, Bo Qiu, for his assistance with this research. I am grateful for all the assistance of Shuiming Chen who helped me with MATLAB and analyzing the figures that I plotted. Finally, I would like to thank the current GES chair, Jane Schoonmaker, for providing a great opportunity to experience scientific work.

ABSTRACT

The structures of warm-core eddies and cold-core eddies were studied in the Northwestern region of the Hawaiian Islands. The study area extends from 180 ˚ W to 140 ˚ W in the zonal band 21˚N to 35˚ N. The variability of the sea surface height (SSH) was derived from the combined mission of TOPEX/Poseidon and ERS altimeters during the period between October 1992 and January 2004 and used to visualize the natures of several eddies generated in this region. Warm-core and cold-core eddies have been traced on maps with the altimeter observations every seven days. Emphasis was placed on the investigation of the spatial and temporal contexts for warm-core and cold-core eddies. It was found that both the warm and cold-core eddies propagated westward in the study area, and the propagation speed has been estimated as 3.25 cm/s. It was also discovered that the warm-core and cold-core eddies were generated by the baroclinic instability in the Subtropical Frontal Zone (STFZ), which is located at 28˚ to 30˚N, and that most of the eddies were observed to disappear along the islands. Eddies were affected by bottom topography in the vicinity of Hawaiian Ridge. In particular, the sea floor shallower than the depth of 1000 meters blocked mesoscale eddies. Finally, the Eddy Kinetic Energy (EKE), horizontal temperature distribution within warm-core eddy and cold-core eddy, and the relationship between eddy propagation speed and latitude were all investigated.

TABLE OF CONTENTS

LIST OF TABLES

Page

LIST OF FIGURES

List OF ABBREVIATIONS

AVISO	Archiving, Validation and Interpretation of Satellite Oceanographic data
CLS	Collecte Localisation Sattelites
CNES	Centre Nationale d'Etudes Spatials
Envisat	Environmental Satellite
ERS	ESA Remote-Sensing Satellite
ESA	European Space Agency
MSLA	Maps of Sea Level Anomalies
NASA	National Aeronautics and Space Administration
Ssalto	Segment Sol multimissions d'ALTimétrie, d'Orbitographie et de localisation
RMS	Root Mean Square
SSH	Sea Surface Height
SST	Sea Surface Temperature
TMI	TRMM Microwave Imager
TOPEX	Ocean Topography Experiment
TRMM	Tropical Rainfall Measuring Mission

1. INTRODUCTION

1.1. Mesoscale Eddy

Mesoscale eddies are energetic circulations about 250 km in width and are found almost everywhere in the ocean (Ebuchi and Hanawa, 2001; Rhines, 2001). Eddies are generated in the way similar to when you stir a bathtub filled with water, whirling and unstable circulations come up to the water's surface. Mesoscale eddies are generally created from the instabilities of major currents over short time period (Rhines, 2001). The role of eddies is known to transport heat energy, trace chemicals, and nutrients across the ocean. Biological communities can be affected tremendously by eddies. Eddies can also be responsible for vertical movements that can reach 5 kilometers downward (Rhines, 2001).

There are several sources of mesoscale eddies in the ocean. Some are generated directly by winds or cooling at the water's surface. Some are from mixing, waves of smaller scales, or the bottom topography of the ocean (Rhines, 2001). It is also said that both barotropic and baroclinic instability are the dominant processes of eddy formation (Jakobsen, 2000). In the idealized situation, seawater is considered to have constant density. In this situation, the surfaces of equal pressure, the isobaric surfaces are parallel to the sea surface. If ocean water is well-mixed horizontally, density increases with depth. Thus, the sea surface is also parallel to the surfaces of constant density, isopycnic surfaces. When the isobaric surfaces are parallel to isopycnic surfaces and the sea surface, such conditions are called barotropic. If there are lateral variations in density and isobaric surfaces are no longer parallel to isopycnic surfaces, this condition is called baroclinic. The horizontal shear velocity associated with the path of barotropic flows influenced by the bottom topography could lead to barotropic instability and the formation of mesoscale eddies (Jakobsen, 2000).

Mesoscale eddies in the Northwestern region of the Hawaiian Islands were traced by using Sea Surface Height (SSH) anomaly derived from the combined TOPEX/Poseidon and ERS-1 and 2 altimeters for the period from October, 1992 to January, 2004. The study area is located at 180 ˚ W to 140 ˚ W in the zonal band 21˚N to 35˚ N (Figure 1). The SSH date derived from the mission by Collecte Localisation Sattelites (CLS) is instrumental in investigating the spatial and temporal evolutions of the mesoscale eddies. The altimetry data used in this study played a crucial role in analyzing Eddy Kinetic Energy (EKE), the structure of the eddies, the eddy propagation, horizontal temperature distribution over the warm-core and cold-core eddies, and the correlation between the propagation speed of eddy and latitude. Mesoscale eddies are classified into warm-core (Figure 2 (a)) and cold-core (Figure 2 (b)) eddies by the direction of their rotation. This study analyzed 12 warm-core and 13 cold-core eddies totaling 25 eddies in the Northwestern region of the Hawaiian

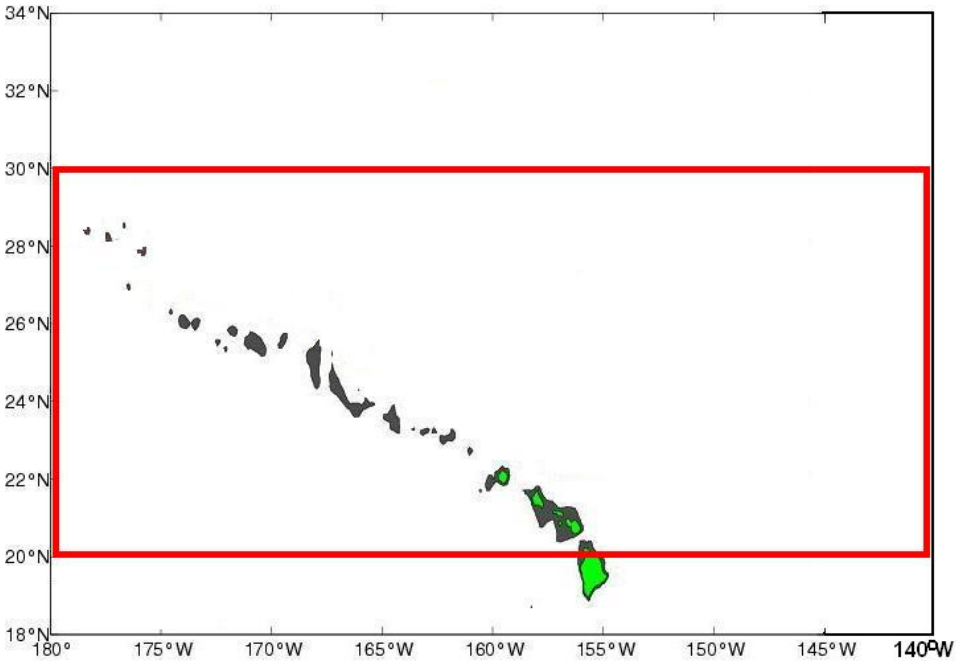

Figure 1: The area enclosed by red line is the study area. It extends 180 ˚ W to 140 ˚ W in the zonal band 21˚N to 35˚ N.

Islands. Both of the warm-core and cold-core eddies are similar in terms of the frequency of occurrence, shape, diameter, and intensity. Warm-core eddies are known to rotate clockwise in the Northern hemisphere, while cold-core eddies rotate counter clockwise. The centers of warm-core eddies are typically warmer than their peripheral region and downwelling occurs at their centers. Thus warm-core eddies are associated with nutrient deficient water. Cold-core eddies rotating in the Northern hemisphere can bring cold and nutrient-rich water to the surface by upwelling at their centers. Cold-core eddies can be a biologically productive spot. The water at the center of cold-core eddy is generally colder than that of the surrounding water. Furthermore, the temperature of the water within the eddy is generally different from that of the surrounding water and local weather can also be influenced by the eddy (Perkins, 2003).

1.2 Horizontal Structure of Mesoscale Eddies

The Coriolis force and buoyancy force are important in discussing the physical property of eddies. Buoyancy force is determined by both the water temperature and salinity. Buoyancy makes the ocean layered such that dense water overrides dense water. The Coriolis force changes the motion of the oceans and atmosphere, and is measured by $2\Omega \sin(\theta)$, where Ω is the angular velocity of the earth (7.29×10^{-5} per second) and θ is the latitude. We usually denote:

$$f = 2\Omega \sin(\theta) \tag{1}$$

where f is called the Coriolis parameter. For a particle with mass m moving with speed u, the expression becomes:

$$\text{Coriolis force} = m \times 2\Omega \sin(\theta) \times u \tag{2}$$

In addition, buoyancy force is a measure of the buoyancy frequency and it influences the eddy's vertical structure. The buoyancy frequency, N, is measured in

radian per second. N is defined when a region of the ocean's water is lifted up and released as the number of oscillations per unit time.

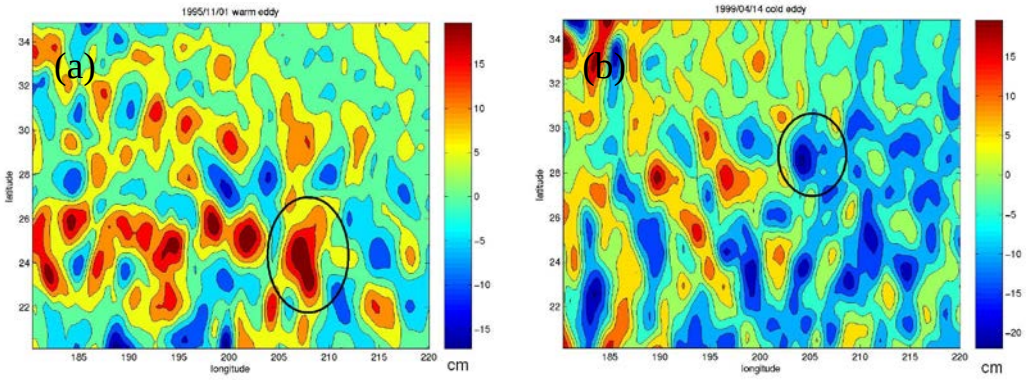

Figure 2: Maps of the SSH anomaly fields (November 11, 1995, and April 14, 1999). Contour interval is 5 cm. Red and blue represents positive and negative anomalies, respectively. The encircled regions in (a) and (b) show examples of a warm-core eddy and a cold-core eddy, respectively.

The diameters of mesoscale eddies are calculated by equation (3) assuming that the buoyancy forces and Coriolis forces are similar in magnitude. In this case, the width λ is calculated by:

$$\lambda = NH/f \tag{3}$$

In the above equation, f and N are already defined in equation (1) and (2), and H is the vertical scale of the mesoscale eddy. As the above expression indicates, λ becomes smaller with increasing latitude. λ ranges from 10 kilometers at high latitudes to hundreds of kilometers in the tropics (Rhines, 2001).

1.3 Mesoscale Eddies and Net Primary Production

The counter clockwise rotation of cold-core eddies leads to upwelling at their center. This upwelling is also called eddy pumping. Cold nutrient-rich water is pumped toward the ocean surface. Cold-core eddies thus tend to be biologically productive areas. The study of cold-core eddies is useful because it could provide beneficial information regarding fishery activity. The cold-core eddies that can scoop

up nutrient-rich water from the abyss rotate in counter clockwise in the Northern hemisphere and opposite in the Southern hemisphere. Phytoplankton can flourish with sufficient nutrients within the cold-core eddies. According to Sakamoto et al (2004), eddy pumping and thermocline uplift by 1000 meters may lead to the increased production of microorganisms in the euphotic zone. The thermocline uplift will be further discussed in section 5.2. Consequently, the populations of marine organisms such as zooplankton and fish are increased in the surface water. It is also found that the nutrient injection to the surface water is associated with increased primary productivity and increased Chlorophyll a levels that indicate the increased production of photosynthetic organisms (Sakamoto et al., 2004).

Such phenomenon draws the attention of fishermen. For example, in the early 1990s, a surface Hawaii-based fishery for swordfish started in the central North Pacific, which is the region north of the Hawaiian Islands (Seki et al., 2002). The region where many swordfish are found is known as the Subtropical Frontal Zone (STFZ). The STFZ is occupied by cold-core eddies to the north and warm-core eddies to the south (Seki, and et al, 2002). The area of high concentration of nutrient inputs corresponded with STFZ, and the highest catch rates of swordfish were also found in the same region (Seki et al., 2002). Thus, the study of eddies is also useful in maximizing the fish catch.

1.4 Mesoscale Eddies and Heat Transport

Eddies are an important process as a major transporter of ocean heat because eddies contain large kinetic energy compared to the average ocean circulation (Roemmich et al., 2001). Eddies in this study have traveled an average distance of 450 km. It could be enough distance for the heat transport process of eddy to affect the local climate. Research suggests that SSH is strongly related to the thermocline

depth; high SSH corresponds downward thermocline (Jacobs et al., 2001). This mechanism will be discussed in detail in section 5.2.

2. DATA

2.1 TOPEX/Poseidon Altimeter

SSH derived from satellite altimetry has long been provided information on the study of ocean circulation (Jacobs et al. 2002). The TOPEX/Poseidon satellite altimeter (Figure 3) has been one of the most useful sources of SSH information (Mitchum, 1995). The TOPEX/Poseidon satellite was launched in 1992 to measure the global ocean SSH with unprecedented accuracy (Sakamoto et al., 2004). This project started as a joint mission between the United States National Aeronautics and Space Administration (NASA) and the French Centre Nationale d'Etudes Spatials (CNES) agencies. The mission is to determine how global ocean circulation behaves and to understand the interaction of the ocean with the atmosphere. The altimeter makes sea level measurements with accuracy better than 10 cm (Mitchum, 1995). The TOPEX/Poseidon altimeter flies at an altitude of 1330 km, inclined at 66 degrees to the Earth's axis (AVISO/altimeter, 1996). The altimeters cover a set of ground-tracks (Figure 7). The points where the ground-tracks cross each other are called crossovers. The satellite repeats a global set of ground-tracks every 10 days. The study area is from 20° to 35° N and from 140° to 180° W, which coincides with the Northwestern region of the Hawaiian archipelagoes including the vicinity of the Hawaiian Ridge. Radar altimeters on board the satellite transmit signals at high frequency (over 1700 pulses per second) to the Earth, and receive the reflected signals from the surface ocean (AVISO/altimeter, 1996). The travel time of the signal between the satellite and sea surface is measured, and the estimates are averaged over second. However, one problem is that when electromagnetic wave travels through the atmosphere, the signals are intervened by water vapor or by ionization. One solution to this problem is to estimate the index of refraction. (Mitchum, 1995)

Figure 3: TOPEX/Poseidon Altimeter

2.2 Jason-1 Altimeter

Jason-1 (Figure 4) was launched in December, 2001 and was designed to follow the TOPEX/Poseidon. It continues to provide data of the same quality as the TOPEX/Poseidon. Jason-1 is a smaller and cheaper satellite compared to the TOPEX/Poseidon. All the instruments on board Jason-1 are derived from those on TOPEX/Poseidon. Jason-1's instruments and data processing systems are constructed based on the lessons learned from the TOPEX/Poseidon. The measurement conducted by Jason-1 is mainly focused on ocean SSH all over the globe, telling us more about deep-water circulation (Aviso/Altimetry, 1996). The satellite's orbit is identical to the TOPEX/Poseidon.

Figure 4: Jason-1 satellite altimeter

2.3 ERS (ESA Remote-Sensing Satellite) -1 and 2 Altimeters

ERS-1 and ERS-2 altimeters (Figure 5) make the measurement of earth's atmospheric and surface properties using microwaves. ERS-1 was launched in July, 1991 from Guiana Space Center by the European Space Agency (ESA), and it flies at an altitude of 780 kilometers (AVISO/altimeter, 1996). ERS-2 was launched 24 hours after ERS-1, and has similar instruments as ERS-1. ERS-2 makes a complete orbital cycle in 35 days, which is one day longer than ERS-1 (AVISO/altimeter, 1996). Both ERS systems maintain the ground-tracks within 200 meters (AVISO/altimeter, 1996).

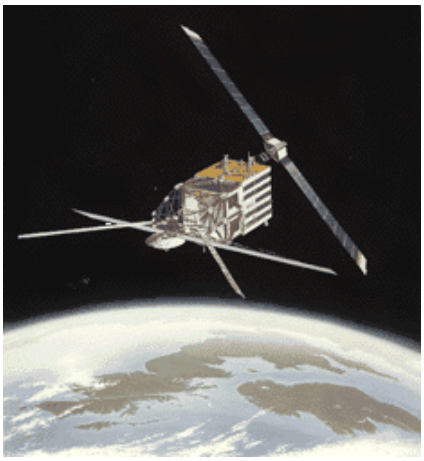

Figure 5: ERS-1/2 satellite altimeter

2.4 Envisat (Environmental Satellite) Altimeter

The Envisat Altimeter (Figure 6) was launched March, 2002 as the follow-up of ERS-1 and 2 (AVISO/altimeter, 1996). It flies at an altitude of 800 kilometers (AVISO/altimeter, 1996). It is devoted to environmental studies, and its mission is to observe the Earth's atmosphere and surface providing near-real time data sets. Its orbital period is 35 days, which is similar to ERS-1 and 2 (AVISO/altimeter, 1996).

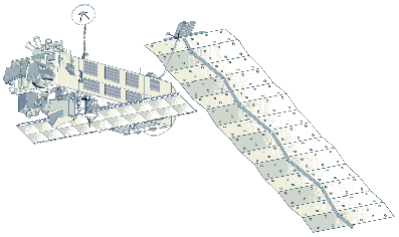

Figure 6: Envisat Satellite Altimeter

2.5 Multimission Altimeter Products

The multimission altimeter products were developed by Collecte Localisation Sattelites (CLS) as part of the Developing Use of Altimetry for Climate Studies (Duacs) (AVISO/altimeter, 1996). Duacs greatly helped the development of the near real time system necessary for operational oceanography and climate forecasting projects. A new version of the system led to significant improvements in the processing algorithms and the data processing of TOPEX/Poseidon, Geosat Follow-on, Jason-1, and Envisat. ERS-2 data are not available after June, 2003 (AVISO/altimeter, 1996). The new system is known as Ssalto/Duacs. The system resolved a major pre-existing problem in the precision of the data sets. The problem is that a satellite that revisits the same point frequently covers fewer points than a satellite that has a longer orbital cycle. Operating several satellites together was the answer to this problem.

An example of combinations is multioperation of TOPEX/Poseidon or Jason-1 and ERS-1/2 or Envisat. TOPEX/Poseidon and Jason-1 are designed to complete one cycle per 10 days. Their ground-tracks are spaced by approximately 315 kilometers at

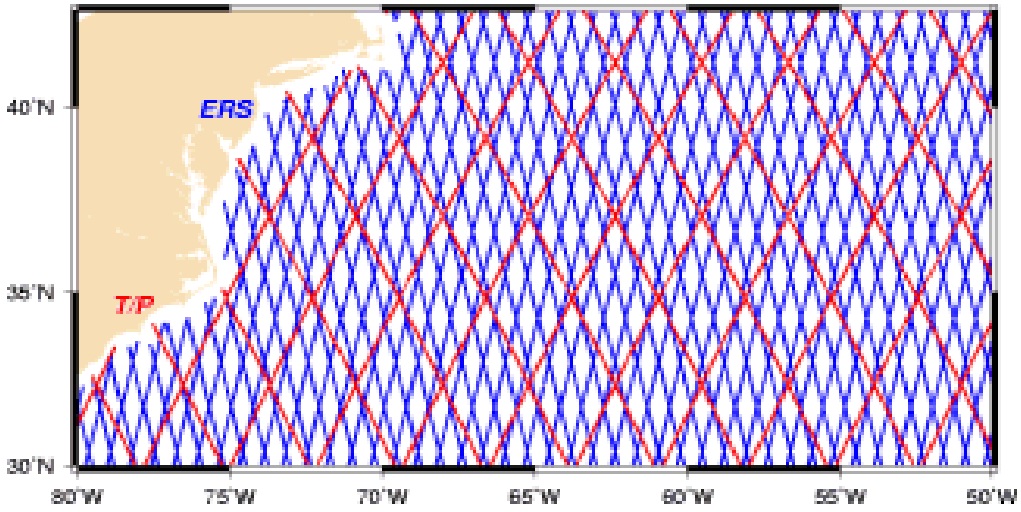

Figure 7: TOPEX/Poseidon pass over the same point frequently, but their ground-tracks are 315 kilometers apart. On the other hand, ERS-1/2 revisit the same point less frequently than TOPEX/Poseidon, but the space between ground tracks are just 80 kilometers. Blue lines and red lines represent the path of ERS-1/2 and TOPEX/Poseidon, respectively.

the equator (AVISO/altimeter, 1996). On the other hand, ERS-2 and Envisat only pass over the same point every 35 days, and the space between the tracks at the equator is about 80 kilometers (AVISO/altimeter, 1996). Figure 7 shows the difference of ground-tracks between TOPEX/Poseidon and ERS-1 and 2. The combination of altimeters can produce higher resolution maps. High resolution data sets are needed in this study because mesoscale process study requires us to use data with high spatial resolution.

2.6 Sea Surface Height (SSH) Data

In this study, the AVISO Maps of Sea Level Anomalies (MSLA) altimeter products from October 1992 to January 2004 were used. The data sets used in this research are obtained from the combined missions of TOPEX/Poseidon or Jason-1 and ERS-1 and 2 or Envisat altimeters. The data sets were compiled by CLS Space Oceanographic Division of Toulouse, France (Bo and Chen, 2004). They are available every 7 days (AVISO/altimeter, 1996). The maps have 1/3° × 1/3° spatial resolution (AVISO/altimeter, 1996).

The SSH is defined as the difference between the satellite height and the altimetric range.

$$SSH = S - R \tag{4}$$

R is the measurement of distance between the satellite and the ocean surface. The on board radiometer transmits the signal and receives the signals reflected by the ocean's surface. The round-trip time is then measured to calculate the final range, R (AVISO/altimeter, 1996). S is the altitude of satellite, which is tracked in the Doris system developed by CNES. The Doris system accurately measures the velocity of the satellite and the trajectory of satellite (AVISO/altimeter, 1996).

2.7 Sea Surface Temperature (SST) Data

In November 1997, the TRMM Microwave Imager (TMI) radiometer 10.7 GHz on board TRMM satellite was launched to make the measurement of Sea Surface Temperature (SST) (Remote Sensing Systems, 2004). The measurement of SST through clouds has been a difficult challenge for many years. The microwave of 10.7 GHz made it possible to travel through clouds (Remote Sensing Systems, 2004). The surface ocean with cloud cover can now be viewed with the TMI radiometer. The important advantage of microwave retrievals is that they are not affected by aerosols and water vapor in the atmosphere. However, microwave retrievals are susceptible to surface roughness, while infrared radiometer retrievals are not. Combining the micro wave retrievals with radiometer retrievals, TRMM satellite SST measurement finally removed the effect of surface roughness. For this study the 1 week mean SST product on a 1/4° × 1/4° grid was used. The products cover the period from November 1997 to the present.

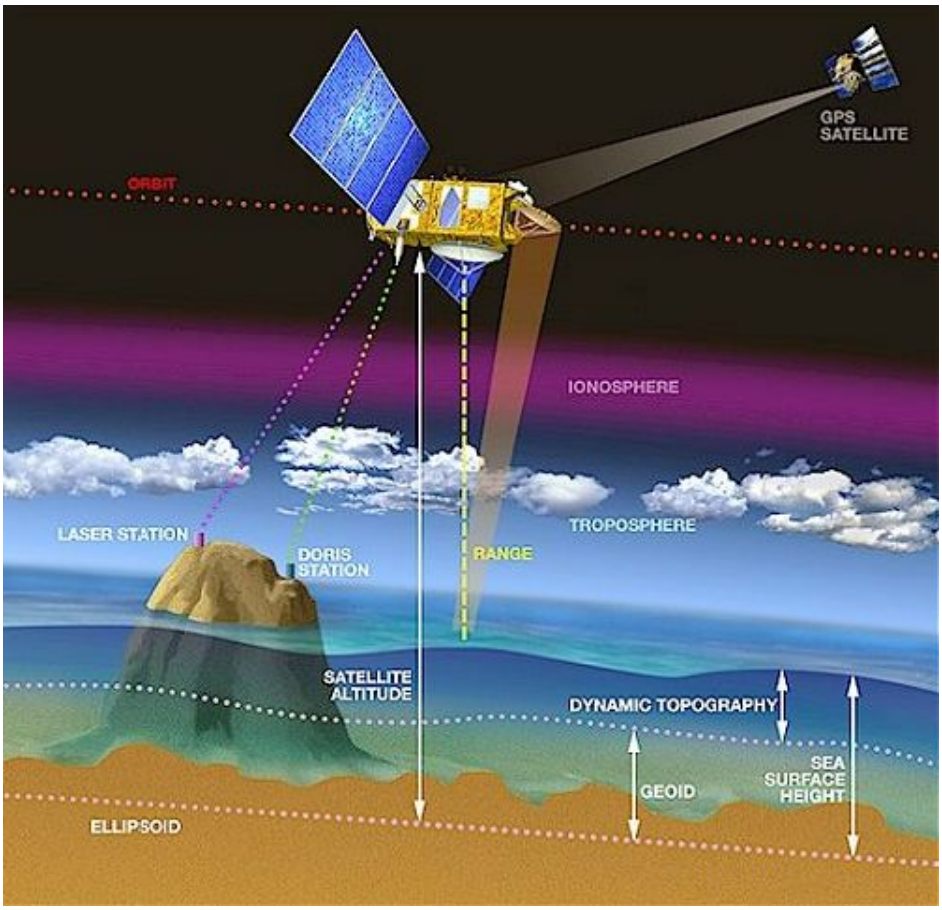

Figure 8: The range, R between satellite and ocean's surface is determined by the transmitted signals that are sent toward ocean's surface. The signals are reflected by the ocean, and the round-trip time of the signals are measured. The travel time is eventually converted to the range between satellite and ocean. The range is subtracted by a satellite altitude, deducing SSH.

3. METHOD

3.1 Calculation of Eddy Kinetic Energy (EKE)

The ocean contains both kinetic energy and potential energy. The potential energy of the ocean is about 100 times greater than the ocean's kinetic energy. Eddy kinetic Energy (EKE) refers to the intensity of an eddy expressed as a physical quantity. In this study, the EKEs were evaluated using the following expressions. The SSH data sets derived from the combined mission of TOPEX/Poseidon and ERS-1 and 2 are formatted as:

$$SSH = h(x, y, t) \tag{4}$$

We denote u and v as the eddy zonal velocity component and the eddy meridional velocity components, respectively. The u and v are expressed as follows:

$$u = g/f\,(\partial h/\partial y) \tag{5}$$

$$v = g/f\,(\partial h/\partial x) \tag{6}$$

In the above equations, g denotes the gravity constant which is 980 cm/s² and f is the Coriolis parameter. They are used to evaluate the EKE:

$$EKE = 1/2\,[(u)^2 + (v)^2] \tag{7}$$

EKE calculated in this section is confined to the area from 168˚ to 156˚W in the zonal band between 20.1472˚ and 34.8668˚N. Furthermore, the Root Mean Square (RMS) of EKEs was calculated using:

$$EKE\ RMS = (\Sigma\ EKE^2/n)^{1/2} \tag{8}$$

where n = 586 (From October, 1992 to January, 2004). EKE RMS is mapped in Figure 14 in section 4.3. The time series of EKE was also determined. For the calculation of EKE, I picked one box that has 1/3˚ × 1/3˚ resolution shown in Figure 9.The east-west (x) and north-south (y) slope of the SSH were then calculated using:

$$a = (h2-h1)/3.7106 \times 10^6 \tag{9}$$

$$b = (g2-g1)/3.7106 \times 10^6 \quad (10)$$

$$c = (h1-g1)/3.7106 \times 10^6 \quad (11)$$

$$d = (h2-g2)/3.7106 \times 10^6 \quad (12)$$

where a and b represent east-west slopes, and c and d describe north-south slopes. The velocity in v and u components are calculated by:

$$v1 = (g \times a)/f \quad (13)$$

$$v2 = (g \times b)/f \quad (14)$$

$$u1 = (g \times c)/f \quad (15)$$

$$u2 = (g \times d)/f \quad (16)$$

$$u = \tfrac{1}{2}(u1 + u2) \quad (17)$$

$$v = \tfrac{1}{2}(v1 + v2) \quad (18)$$

The EKE in the time series shown in Figure 15 can be estimated from the above equations.

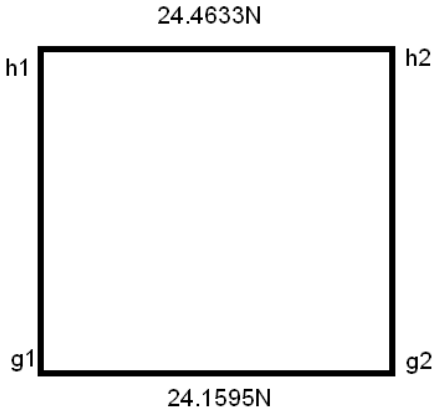

Figure 9: This is a box that has 1/3˚ × 1/3˚ resolution.

3.2 Calculation of Horizontal Temperature Distribution within Eddy

SST data sets derived from TMI radiometer were used in this study. As described in Figure 10, T_1 represents SST at the left side of eddy, and T_3 is SST at the right side of eddy. T_2 and T_4 are SST at the northern side and the southern side, respectively. T_0

is SST at the eddy's center. Ts is estimated as an average of T_1, T_2, T_3, and T_4 in the below equation. In the Figure 10, T_1 can be considered as the head of the eddy, while T_3 can be its tail in terms of the direction of propagation.

$$Ts = (T_1+T_2+T_3+T_4)/4 \tag{19}$$

δT_1 is equal to the difference between T_0 and Ts which is the average of the 4 locations of the eddy. The SST at the center is compared to the peripheral region of eddy:

$$\delta T_1 = T_0 - Ts \tag{20}$$

δT_2 is estimated as the difference between SST at T_0 and T_3:

$$\delta T_2 = T_0 - T_3 \tag{21}$$

δT_3 is determined by subtracting T_1 from T_0:

$$\delta T_3 = T_0 - T_1 \tag{22}$$

Using data sets derived from this subsection, the plots of the time series of δT_1, δT_2, and δT_3 and mean SSH versus δT_1, δT_2, and δT_3 are shown in section 4.4. As a result, distinct features of warm-core and cold-core eddy in terms of temperature distribution can be seen.

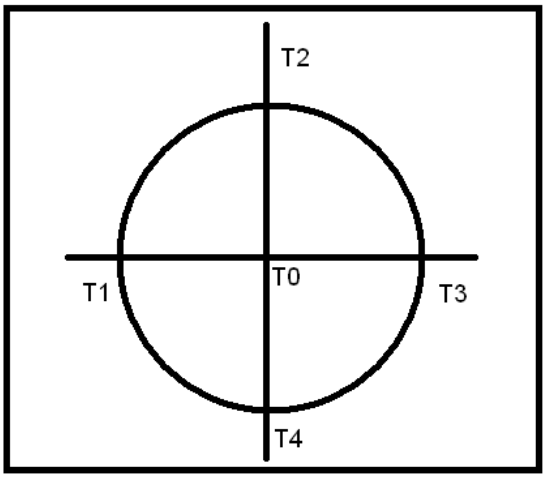

Figure 10: T_0, T_1, T_2, T_3, and T_4 are Sea Surface Temperature (SST) at the location shown in the figure. Because the direction of the eddy propagation is toward the left side, T_1 and T_3 are considered as the eddy's head and tail, respectively.

3.3 Calculation of Theoretical Eddy Propagation Speed with Respect to Latitude

The phase speed of westward propagating eddies is expressed as equations in this subsection.

$$\beta = (2\Omega/r) \cos(\varphi) \tag{23}$$

where β gives the latitudinal gradient of the Colioris parameter, r the radius of the earth (6.3781×10^8 cm), Ω (7.29×10^{-5} radiance per second) the angular velocity of the earth, and φ latitude. The eddy westward propagation speed is a function of latitude, and the theoretical long Rossby wave speed is expressed as:

$$C_R = -\beta c^2/f^2 \tag{24}$$

where C_R is the phase speed of the first mode internal gravity wave. The value of latitude is contained in the Coriolis parameter, f, and in latitudinal gradient of the Colioris parameter, β. Thus it can be said that C_R is inversely proportional to the value of latitude. The discrepancies between observed westward eddy propagation speed and theoretical long Rossby wave speed are further discussed in section 4.4.

4. Results

4.1 An Example of Eddy Tracing

An example of the filtered maps of eddy tracing with the SSH products derived from the TOPEX/Posedion and ERS-1 and 2 altimeters is shown in Figures 2 (a) and (b). The warm-core eddy has a positive SSH anomaly, while the cold-core eddy has a negative anomaly at their center. The average propagation speed was estimated at 3.25 cm/s and the average distance that eddy traveled was 449 kilometers. The average duration of eddy from generation to disappearance was also calculated as 449 days. Table 1 shows average distance traveled, speed, and duration time for warm-core and cold-core eddies separately. Figure 11 shows an example of tracing a mesoscale eddy. Time series of SSH anomalies allows investigation of how eddies develop and disperse. Warm-core eddy which is located at 22.5˚ N to 25.5˚ N in the zonal band of 158˚W to 152˚W was traced. This warm-core eddy progressed westward horizontally. This eddy has traveled over 390 km during a period of about 90 days. The shape, size, and SSH anomaly vary greatly as it progresses westward. The size of the eddy becomes smaller and the circular shape changes over time. The positive SSH anomaly decreases over time. However, it should be noted that the coarse resolution may also affect the shape of the eddy. Because the traced eddy may be within the space between ground-tracks, then the amplitude and the shape of eddy can be reduced and changed, respectively (Ebuchi and Hanawa, 2001).

In this study, only eddies in the region shown in Figure 1 were traced. The Northwestern side of the Hawaiian Islands in the vicinity of the Hawaiian Ridge is an area of unlikely eddy generation (Mitchum, 1995). However, 25 eddies in total at the

Table 1: Comparison of average propagation speed, traveled distance, and duration time between warm-core eddy and cold-core eddy

	Warm-core Eddy	Cold-core Eddy
Average propagation speed	2.65 cm/s	3.84 cm/s
Average traveled distance	300 km	600 km
Average duration time	156 days	180 days

study area were found. The tracing method is described in this section. Only eddies which satisfied the following conditions were analyzed: (1) The duration of the eddy must be at least 3 months (2) Eddies must have a circular shape; the breakdown of circular shape is considered as the end of the eddy (3) Eddies must move. Eddies that did not move were eliminated. At the start of tracing, the likely eddy in circular shape in the filtered SSH anomaly map was chosen, and then the center of eddies was determined by local maximum or local minimum. When the value of the amplitude of eddy is positive, the eddy is considered a warm-core eddy and vice versa. Figure 11 shows an eddy traced during a period from November 22nd to February 2nd. Figure 12 shows the time-series of trajectories and amplitudes of warm-core eddy and cold-core eddy. Local maximum and local minimum exist in warm-core and cold-core eddies, respectively. Both eddies propagate westward. It is also apparent that the amplitudes of warm-core eddy and cold-core eddy decrease (absolute value of SSH decreases towards zero). The trajectories of all eddies are discussed in section 4.2.

4.2 Trajectories of Eddies

Figure 13 shows warm-core eddies and cold-core eddies which are traced using the combined data sets from TOPEX/Poseidon and ERS-1/2. The trajectories of 12 warm-core and 13 cold-core eddies totaling 25 eddies in the Northwestern region of

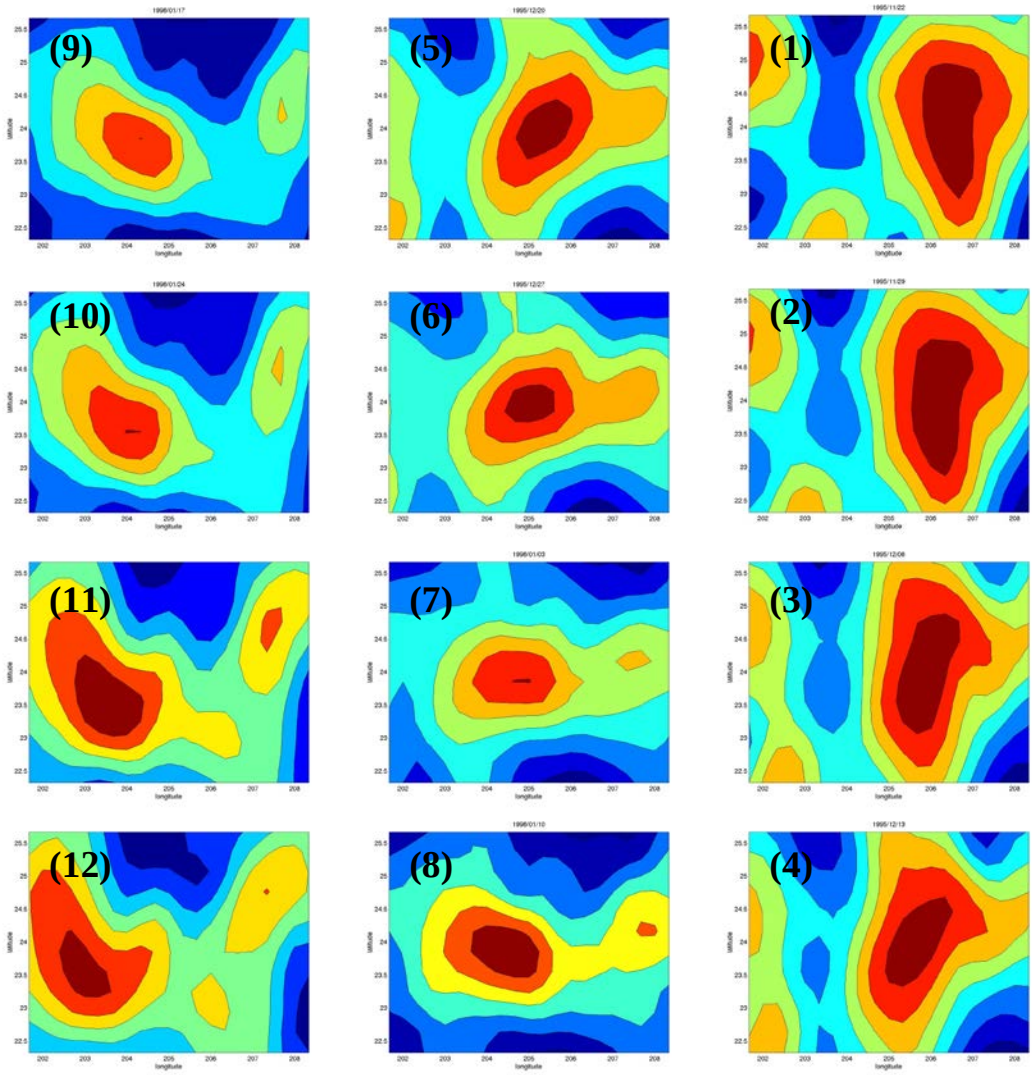

Figure 11: This is an example of tracing warm-core eddy. The tracing of eddy proceed from (1) to (12). This eddy is located at 22.5˚ N to 25.5˚ N in the zonal band of 158˚W to 152˚W and the duration time extends from November 22, 1995 to February 7, 1996.

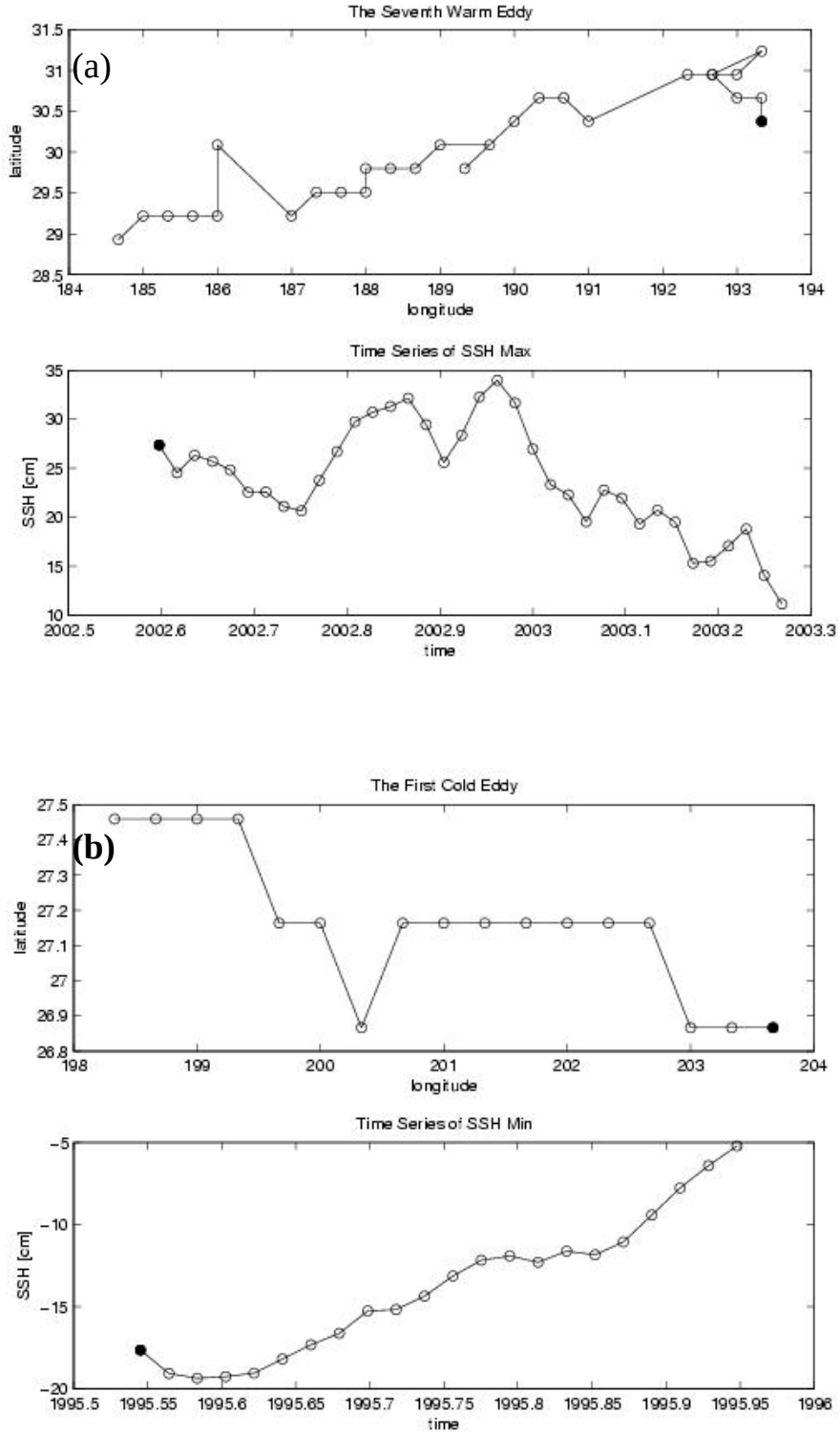

Figure 12: (a) shows a trajectory of a warm-core eddy and time series of SSH anomaly at its center. (b) shows the same features of a cold-core eddy.

the Hawaiian Islands are found in the figure during the period from October 1992 to January 2004. Red dots and lines represent warm-core eddies and blue dots and lines represent cold-core eddies. Most of eddies located at latitude higher than 26˚N seem to bend southward, but eddies detected at 26˚N or lower appears to bend northward as they progress westward. Also, most of the cold-core eddies are tracked in the region between 24˚N and 29˚N, while warm-core eddies are evenly distributed.

The black shaded regions in Figure 13 represent the bottom topography in the vicinity of the Hawaiian Ridge. The depth of the shaded regions is shallower than 1000 meters. In the region around the Hawaiian Ridge, eddies are affected by the bottom topography. No eddies pass over the Hawaiian Ridge in Northwestern regions of the Hawaiian Islands. Warm-core and cold-core eddies went over similar paths. The generation of eddies regardless of whether cold-core or warm-core eddy is located approximately in the zonal band between 22˚N and 32˚N. Eddy at latitude between 32˚N and 35˚N was not found, and longitude between 145˚W and 140˚W. Off the west coast of the Big Island, some eddies were detected, but the lifetime of these eddies were too short to be traced and they did not move. On the other hand, most of the breakdown of eddies occurred relatively close to the east coast of the Hawaiian Islands and the eastern edge of the shaded basin.

4.3 Eddy Kinetic Energy (EKE)

Figure 14 shows the distribution of mean EKE in the Northwestern region of the Hawaiian Islands. The high EKE region is restricted to the zonal band of 24.5˚N and 27˚N between 167˚W and 162˚ W. The region of the second largest EKE is in the zonal band of 24.5˚ N and 25.7˚ N between 161˚ W and 159˚ W. This distribution follows the equations calculated in section 3.1. High values are associated with greater velocity of mesoscale eddies. We see the high eddy activity in the region

colored yellow green and light blue. The distribution of EKE is concentrated in the region off the Emperor seamounts. This region corresponds to where most of the cold-core eddies are found in this study. Two regions are considered as big pools of eddy activity. Very low eddy activity is observed in the ocean far off the coast of the Hawaiian Islands and seamounts (Figure 14). The region colored blue corresponds to EKE values less than 200 cm^2/s^2. In contrast the region colored light green is equivalent to EKE values higher than 300 cm^2/s^2. However, EKE values higher than 400 cm^2/s^2 were not found in this region. Figure 15 (a) shows the time series of EKE during the period from October, 1992 to January, 2004. The annual cycle is not seen in this figure, but its amplitude repeats the oscillations. High EKE is observed in 1993, 1998, the end of 2002, and 2004. Minimum EKE levels continued from 1992to 2002. After the highest amplitude value, it goes down below and records the lowest value. This cycle is repetitive throughout the years. On the other hand, Figure 15 (b) and (c) describe the time series of the velocity in the v and u components. Both u and v oscillate repetitively as EKE does.

4.4 Temperature Distribution over Warm-core and Cold-core Eddy

Figure 16 (a) and (b) are examples of temperature distributions within warm-core and cold-core eddies, respectively. Figure 16 shows the time series of temperature at the center of the eddies, T_0 shown in Figure 10, and the time period of temperature is equivalent to the duration of the traced eddies. The δT_1 of warm-core eddy is relatively positive. In both summer and winter time, the warm-core eddy maintains higher temperature at its center than its surrounding region. The change in δT_2 is similar to δT_1, and the temperature at the eddy center tends to be warmer

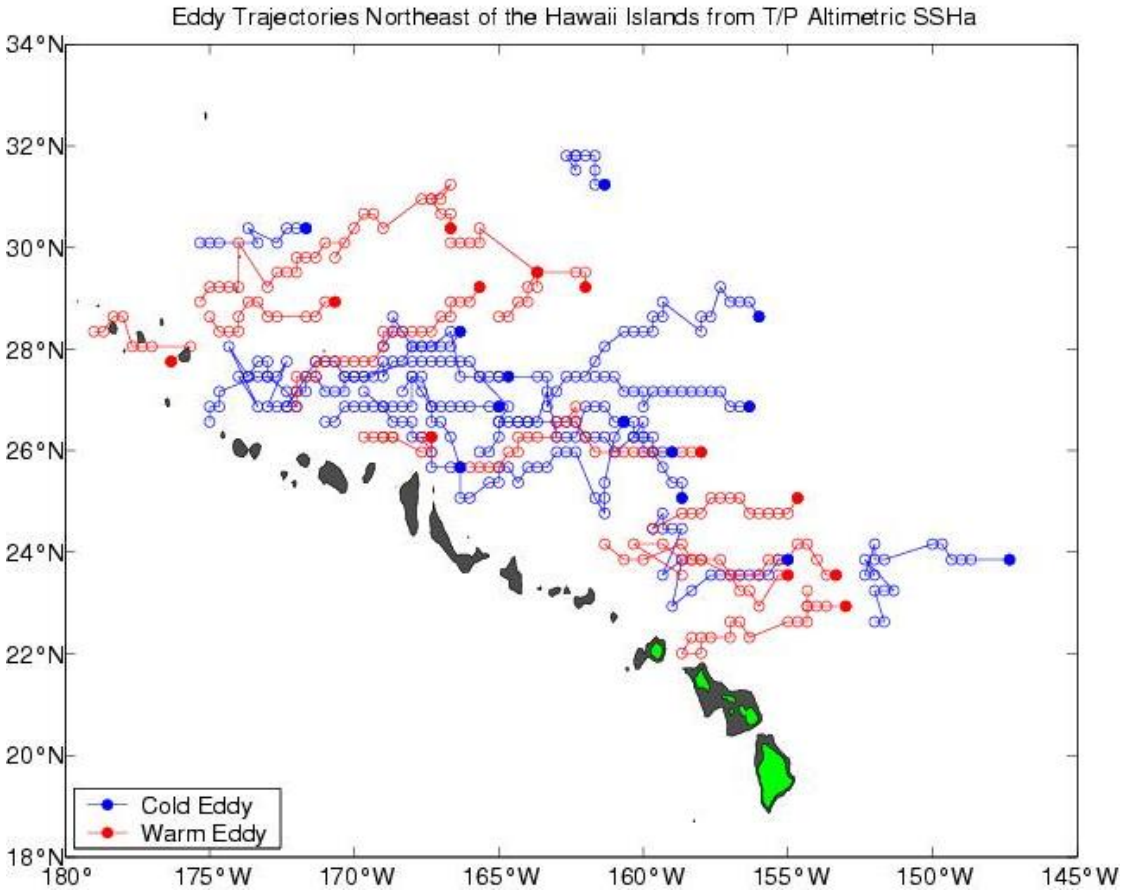

Figure 13: The shaded regions are bottom topography in the vicinity of the Hawaiian Ridge. Blue dots and lines denote the path of cold-core eddies and red dots and lines warm-core eddies. The green colored Hawaiian Islands comprise the islands of Kauai, Oahu, Molokini, Maui, and Hawaii from west to east.

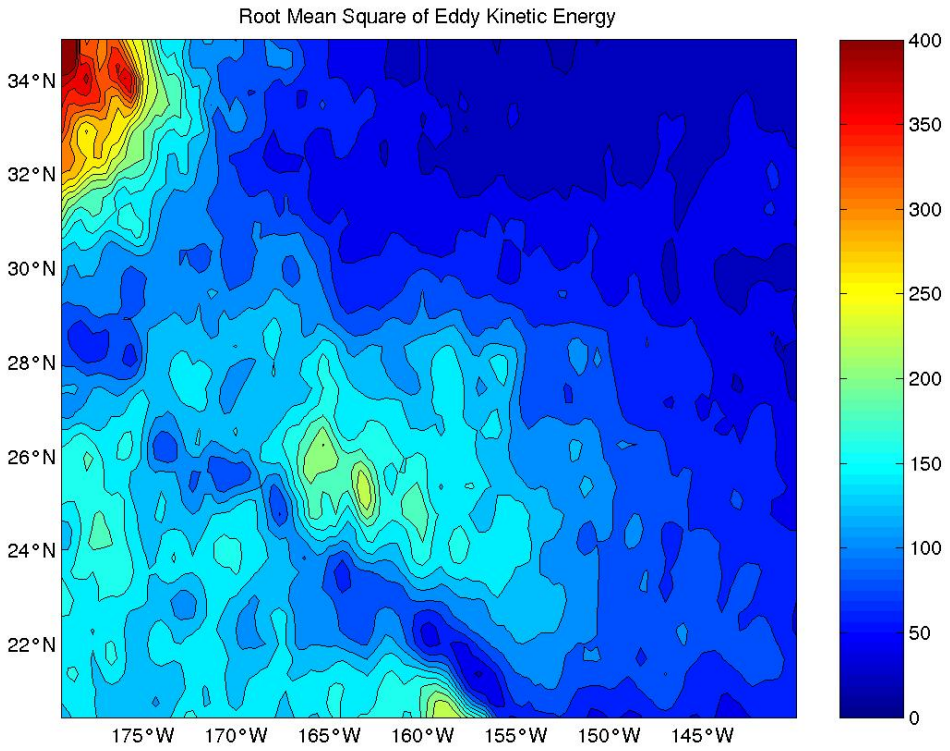

Figure 14: Map of the EKE mean in the Northwestern region of Hawaiian Islands. Based on data derived from the combined mission of TOPEX/Poseidon and ERS1/2 altimeter from October 1992 to January 2004, EKE is expressed as a contour map, and unit is cm^2/s^2. Contour interval is 50 cm^2/s^2.

than its tail. However, δT_3 presents different trend compared to other δTs. δT_3, the temperature difference between the eddy's center and head was observed to remain relatively negative. Water in the eddy's head region is warmer than its center.

As for cold-core eddies, the δT_1 is found mainly in the negative zone. This indicates the water in the eddy's center tends to be colder than its peripheral regions. Similarly, δT_2 also shows negative values (Figure 16). The water within the cold-core eddy is colder than water in its tail region. δT_3 oscillates greater than δT_1 and δT_2. It changes sharply in the way that it has both high positive mark and low negative mark. However, it tends to be observed in negative side.

In Figure 17, the temperature distributions within 16 eddies (7 warm-core and 9 cold-core eddies) have been observed to statistically determine the temperature profiles of the surface water. A majority of δT_1 of cold-core eddies are negative, while δT_1 of warm-core eddies are concentrated along the zero line (Figure 17 (a)). δT_1 remains positive, but on a larger scale it experiences no change. Thus the water at the center of the warm-core eddies has almost the same temperature as the water in its surrounding region. The δT_2 of warm-core and cold-core eddies clearly presents distinct features between them (Figure 17 (b)). All δT_2s of cold-core eddies are negative. Conversely, those of the warm-core eddies are positive. This leads to the fact that the water at the center of the warm-core eddies is warmer than the tail region, and vice versa. Finally, δT_3s in Figure 17 (c) show interesting result. A majority of δT_3 of cold-core eddies have been found in positive side, and all of δT_3 of warm-core eddies in the negative side. This indicates that the water at the cold-core eddy's center is warmer than its tail region, while the water of warm-core eddy centers is colder, which will be further discussed in section 5.2.

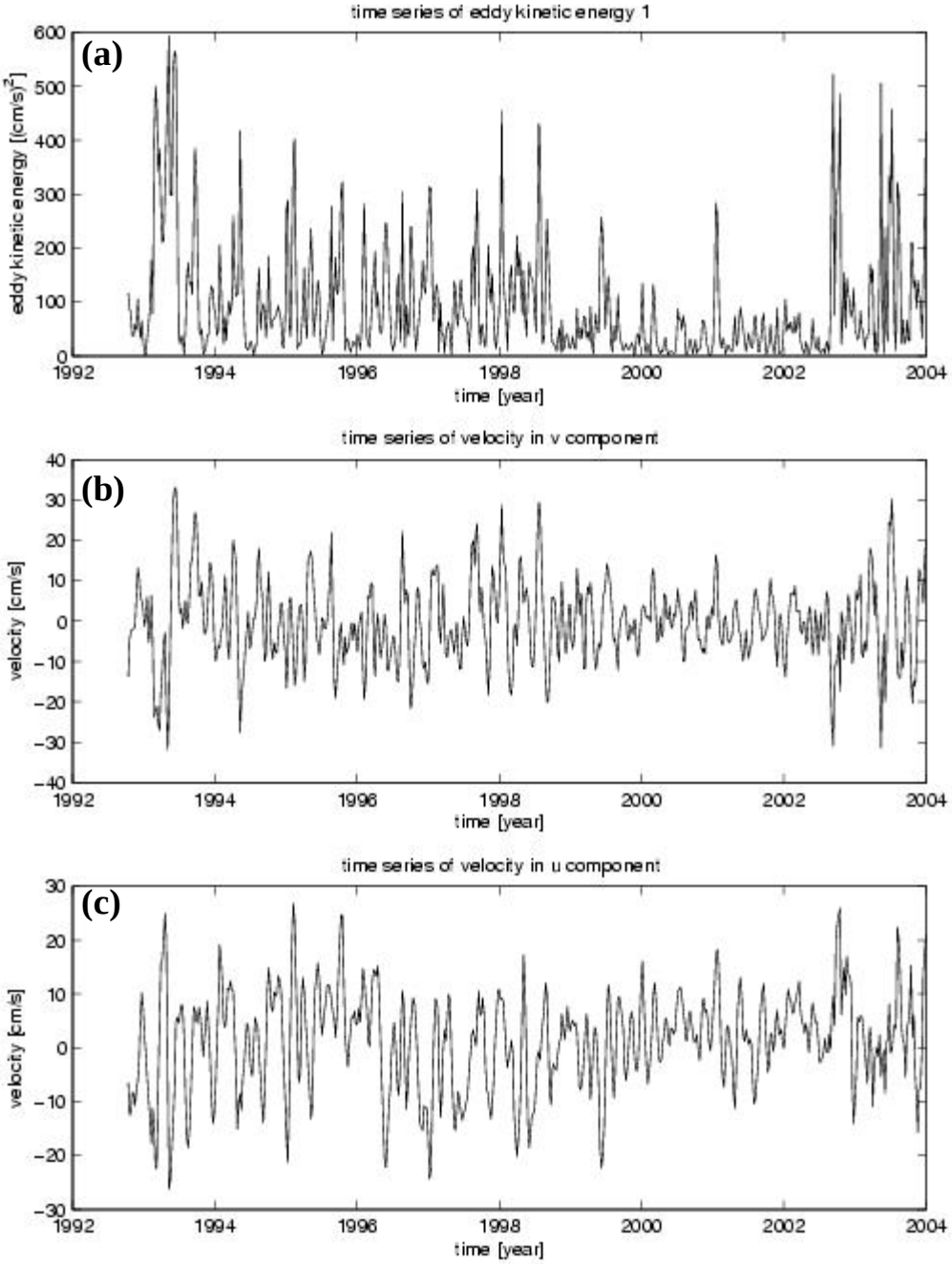

Figure 15: Figure (a), (b), and (c) shows time series of EKE, v component velocity, and u component velocity, respectively. Time is from October, 1992 to January, 2004.

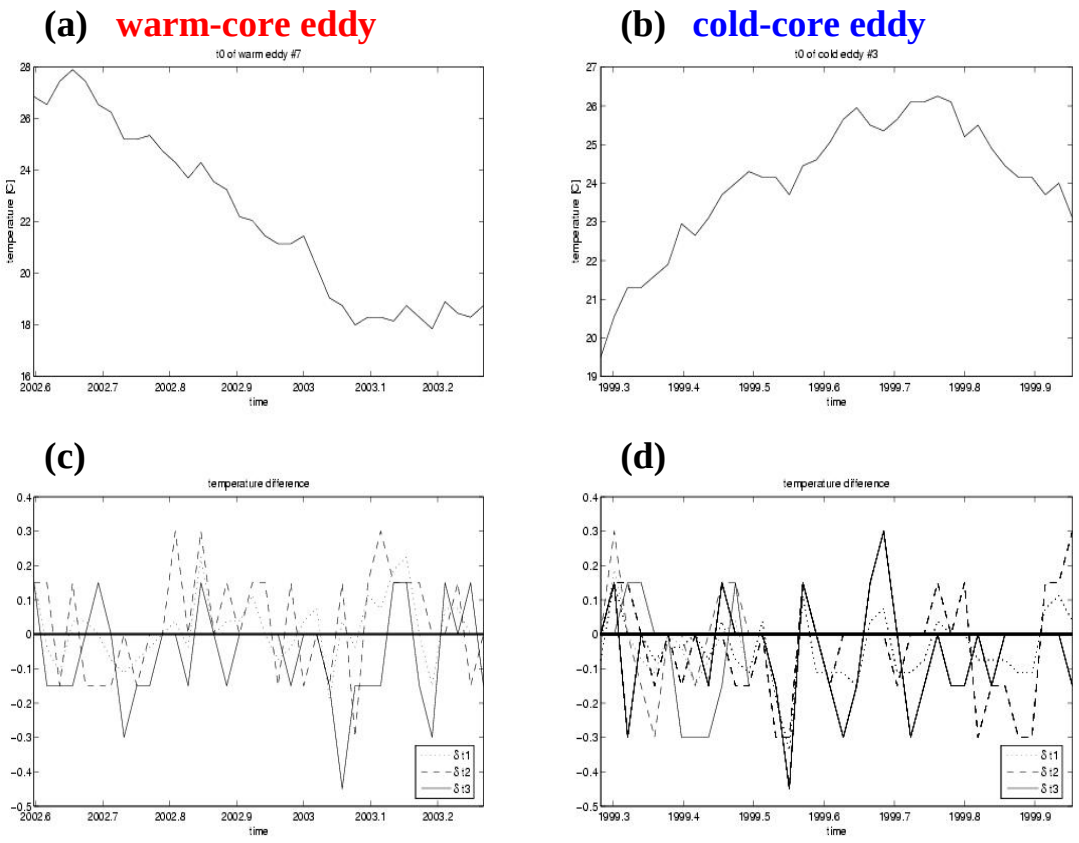

Figure 16: (a) and (b) show the time series of T_0 in warm-core and cold-core eddies, respectively. (c) and (d) show the time series of δT_1, δT_2, and δT_3 within warm-core and cold-core eddies, respectively.

4.5 Correlation between eddy propagation speed and latitude

In Figure 18, the relationship between westward propagation eddy speed and latitude is plotted. In addition, the scattered plots of warm-core and cold-core eddies with respect to latitude are also observed in Figure 18. Warm-core and cold-core eddies are distinguished by different colors and symbols. It can be seen that a majority of cold-core eddies are located between 25˚ and 28˚ N. Warm-core eddies are found in two zonal bands approximately 22˚ - 25˚N and 28˚ - 30˚N.

The theoretical westward eddy propagation speed is determined by equation (24) as described earlier. From Figure 17, robust relationship between westward propagation speed and latitude are presented. As latitude increases, the eddy's propagation speed becomes slower (Figure 18). The negative sign in the propagation speed means 'westward', and positive means 'eastward'. Eastward propagation was not found in this study. Meanwhile, the solid line in the figure is equivalent to the theoretical line calculated (equation (24)). It should be noticed that the scatter plots fit to the theoretical line (Figure 18).

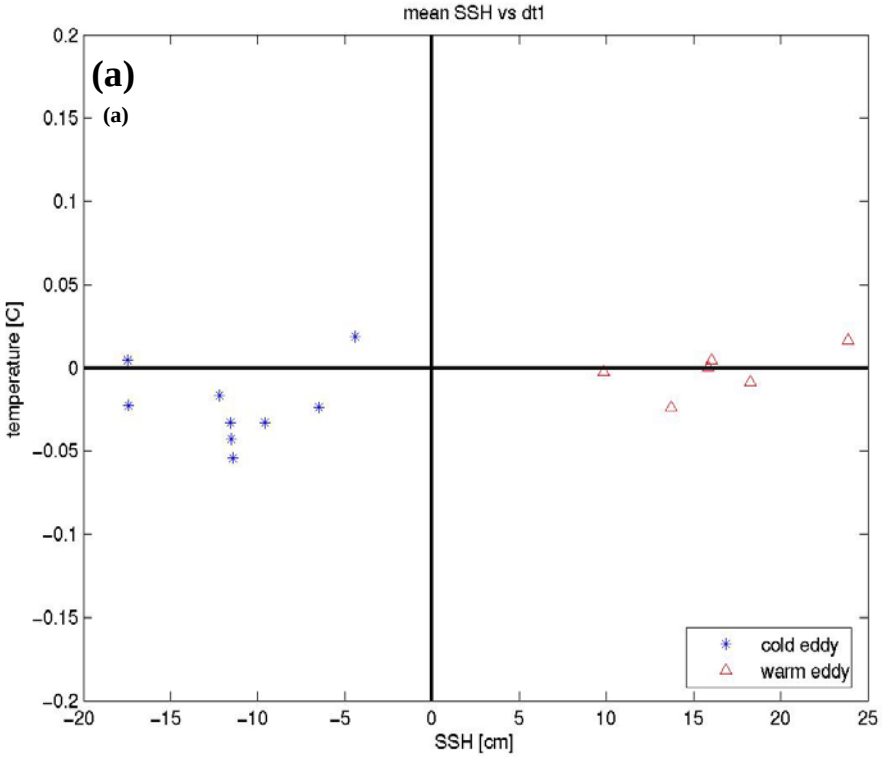
mean SSH vs dt1
(a)
(a)
temperature [C]
SSH [cm]
cold eddy
warm eddy

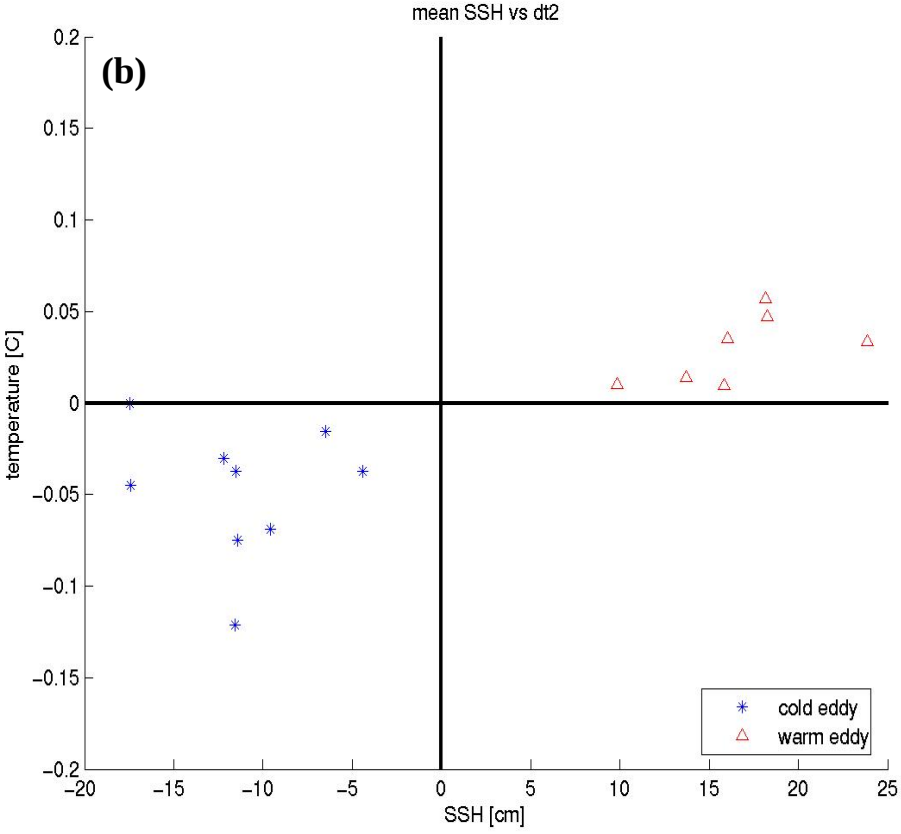
mean SSH vs dt2
(b)
temperature [C]
SSH [cm]
cold eddy
warm eddy

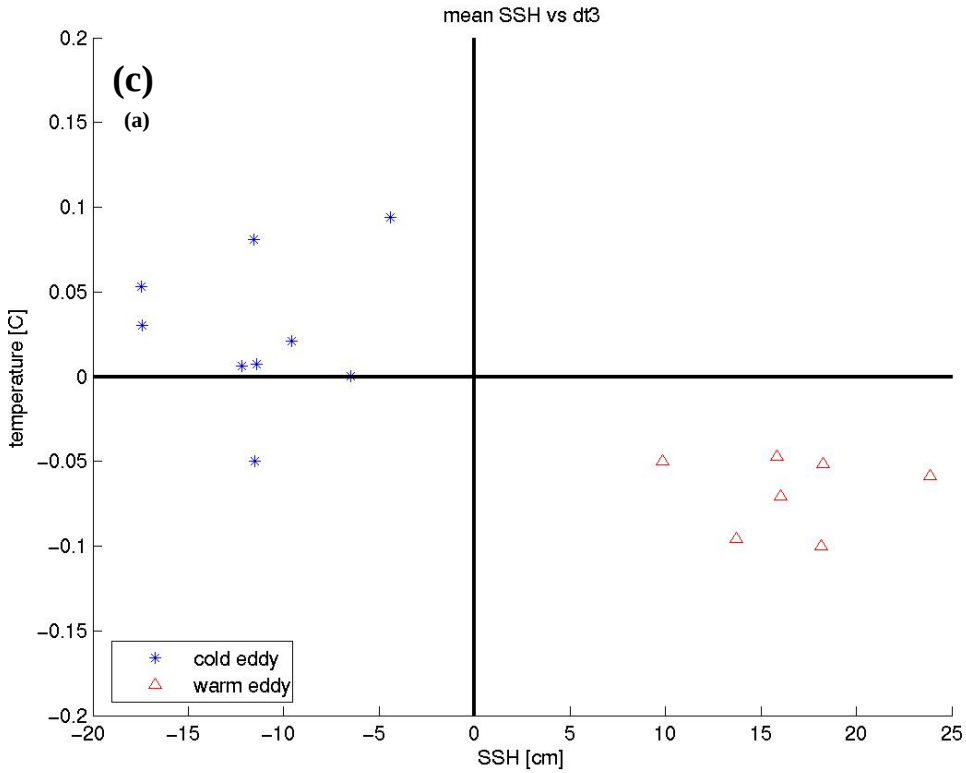

Figure 17: Blue stars represent cold-core eddies, while red triangles represent warm-core eddies. Figure (a), (b), and (c) show the mean SSH versus δT_1, δT_2, and δT_3, respectively.

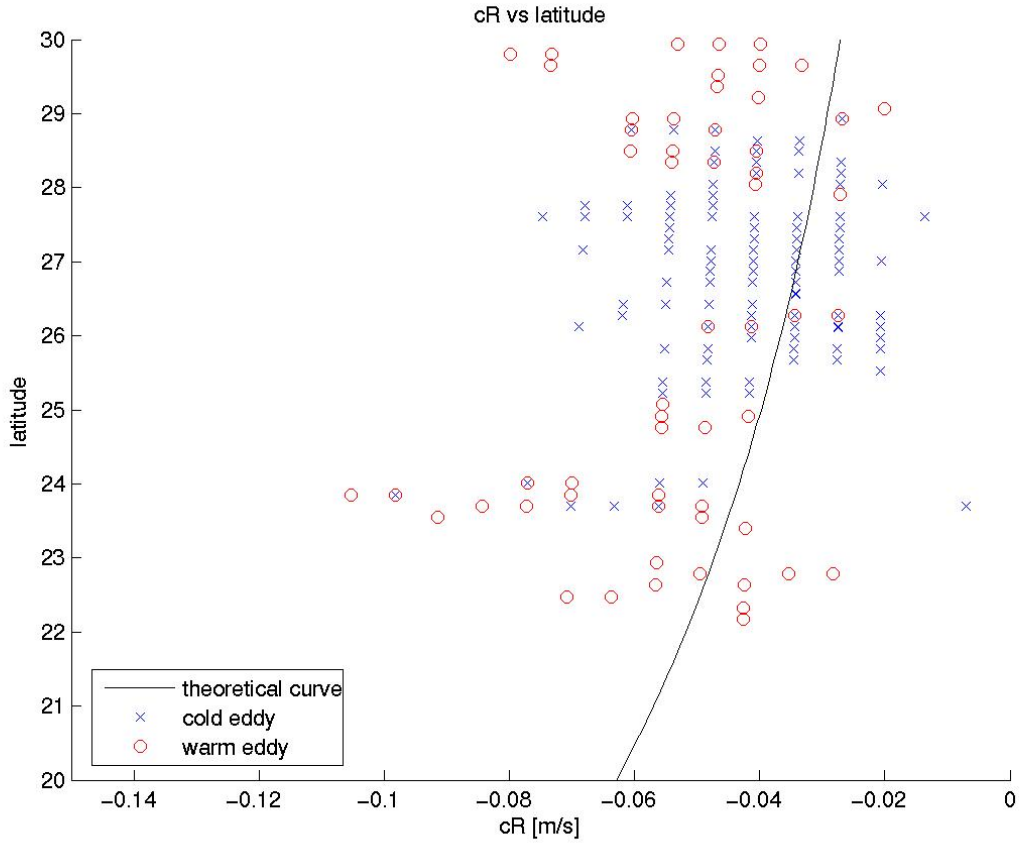

Figure 18: Above figure shows eddy's westward propagation speed versus latitude. Blue x's represent cold-core eddies and red circle the warm-core eddies. The solid black line is the theoretical correlation between westward propagation speed and latitude.

5. Discussion

5.1 Generation and Disappearance Area of Eddies

Annual changes in the Ekman pumping due to the wind stress which occur at the boundary between the trade winds and westerlies may generate mesoscale eddies at about 30˚N (Mitchum, 1995). The boundary tends to fluctuate in the meridional direction. Wind stress at the sea surface leads to vertical motion of surface water via divergence and convergence. When there is divergence of surface water, the surface water elevation increases. Convergence causes the height of the surface water to drop. This effect of vertical displacement of the surface water is called Ekman pumping. However, according to trajectories of mesoscale eddies, most of eddies are generated at the region south to the boundary at which the trade winds and the westerlies meet (Figure 13). This region corresponds to the region where there is a remarkable shear current.

There is more discussion about eddy generation in the STFZ in section 1.3. The region where many swordfish are found is known as the Subtropical Frontal Zone (STFZ), which extends from 28˚ to 30˚N. STFZ is characterized by intensive mesoscale eddy activity (Seki et al., 2002). However, this study shows different tendency of intensive eddy activity area from STFZ. Most of eddies observed in the Figure 13 are prevalent in zonal band 25˚ to 28˚N. This region does not exactly coincide with the STFZ, but mesoscale eddies in Figure 13 seem to be affected by the fronts dominating flow fields in the STFZ. The fronts cause the surface water to be deformed and lead to great instabilities in the region, which may generate mesoscale eddies.

The current that may have caused mesoscale eddies to disappear is discussed below. At first it is noticed that the regions of the disappearance of eddy are close to

North Hawaiian Ridge Current (NHRC) which exists along the Northern coast of Hawaiian Islands. The NHRC coherently flows along the islands at speed of about 0.10 – 0.15 m/s (Qiu et al., 1996). The flow of the NHRC is a narrow band with width of 75- 100 kilometers (Qiu et al., 1996). As the study area is dominated by mesoscale eddies, both the NHRC and mesoscale eddies seem to interact in the region between 22˚ and 25˚N. Eddies detected in such regions appear to bend northward as they progress westward. In addition, gaps exist between the trajectories of eddies and the islands, which corresponds to the narrow band of NHRC along the Hawaiian Islands. Furthermore, EKE maps record high kinetic energy in the zonal band of 24.5˚N and 27˚N between 167˚W and 162˚W. This all suggests that mesoscale eddies merged into NHRC and disappeared. For the regions that are not affected by NHRC, it is apparent that the bottom topography caused mesoscale eddies to disappear. According to Qiu et al. (1996), the Hawaiian Ridge above 500 meters is extremely porous. However, all eddies do not pass over this region. This indicates that eddies have deep roots that can reach more than 500 meters downward regardless of whether they are warm-core or cold-core eddies.

5.2 Eddy Advection Effect

Eddy temperature distributions within warm-core and cold-core eddy are shown in Figure 17. General features of mesoscale eddies are that warm-core eddies and cold-core eddies have warm-core and cold-core, respectively. However, Figure 17 (b) and (c) contradict this fact. The occurrence of warm-core and cold-core eddies are closely related to thermocline where the rapid change in temperature occurs. An important feature of the surface ocean is that variation of SSH tremendously affect the thermocline depth. A sea level variation of 5 centimeters is equivalent to a thermocline displacement of about 50 meters (Chelton and Schlax, 1996). Among the

25 eddies observed in this study, the average height was estimated as 20.9 cm for warm-core eddies, and -15.5 cm for cold-core eddies. In response to this, the depth of the thermocline would change more than 150 m. Thus within warm-core eddies, the thermocline increased in depth and becomes warmer. Conversely, cold-core eddies cause the thermocline depth to decrease in depth. This leads to shallower thermocline depth, and the surface water within the cold-core eddy is cooled by the cold water below the thermocline.

Eddy advection effects need to be applied to this situation. As mentioned in section 1.4, mesoscale eddies are an important natural process as a transporter of ocean's heat, and eddies are able to carry large kinetic energy compared to the general ocean circulation (Roemmich et al., 2001). The most significant eddy heat transport can be detected in western boundary currents, equatorial regions, and the Antarctic Circumpolar Current (Jayne and Marotzke, 2002). Thus, in the region near the equator, such a process is really important because the influence of eddy advection is optimized. Due to the anticyclonic rotation of a warm-core eddy near the equator in the Northern hemisphere, warm water close to the equator is carried northward by the eddy's anticyclonic motion (Figure 19 (a)). The head of the warm-core eddy can then be warmed. The same effect can be applied to a cold-core eddy. A cold-core eddy has cyclonic rotation, and colder water is carried from the northern region to the head region of the cold-core eddy (Figure 19 (b)). This leads to a reverse of the horizontal temperature distribution, and the water at the center of the cold-core eddy becomes colder than at the head of the eddy.

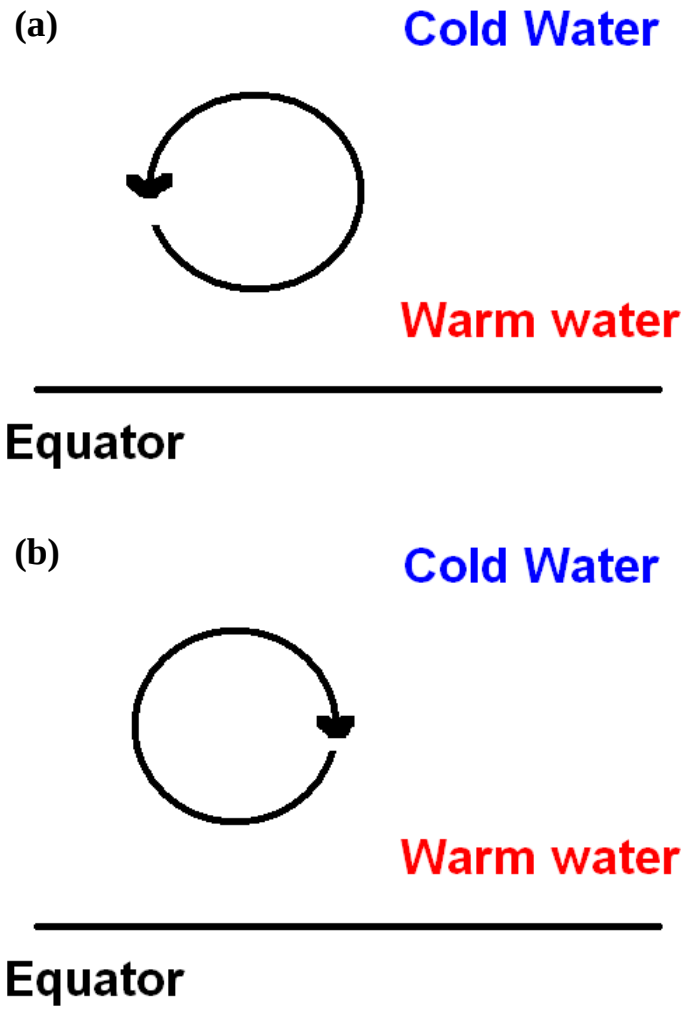

Figure 19: (a) and (b) show the schematic diagrams of the eddy advection effects of warm-core and cold-core eddies, respectively.

6. Conclusion

In present study, I examined the trajectory of mesoscale eddies with the use of altimetric data derived from the combined mission of TOPEX/Poseidon and ERS altimeters. It was found that both warm-core and cold-core eddies propagate westward in the study area. The average propagation speed was estimated as 3.25 cm/s. The westward propagation increases toward lower latitude regardless of whether they are warm-core or cold-core eddies. As shown in Figure 17, data plots seemed to coincide with a theoretical curve.

Mesoscale eddies investigated in this study were either warm-core or cold-core eddies. A warm-core eddy is also called an anticyclonic eddy because of its anticyclonic rotation. As it propagated westward, its height at the center decreased. The average initial height of a warm-core eddy was 20.9 cm. The average duration of a warm-core eddy also estimated as 156 days. On the other hand, a cold-core eddy is also called a cyclonic eddy because it rotates in the same direction as cyclones in the Northern hemisphere. Cold-core eddies also seemed to propagate westward in the same way as warm-core eddy, but their average initial height was estimated as 15.4811 cm. As cold-core eddies propagated, their center height increased until it eventually reached zero height when the eddies died out.

Most of the mesoscale eddies, regardless of whether they are warm-core or cold-core eddies, were generated in the area just south to the STFZ, which extends from 28˚ to 30˚N. The fronts in this region lead to baroclinic instability and cause intensive mesoscale eddy activity. Additionally, the existence and formation of the NHRC along the Hawaiian Islands may have explained the area of disappearance of the eddies. The mesoscale eddies studied in the region between 22˚ and 25˚N seem to merge into NHRC. The mesoscale eddies that disappeared in higher latitude than

25˚N may have been affected by the bottom topography in the vicinity of the Hawaiian Ridge.

Moreover, it was also discovered that analysis of EKE time series in this study area showed its maximum value in 1993 and 2003 and its minimum value in 1999 and 2000 in Figure 15. Those years seem to coincide with the development and evolution of eddies.

The horizontal temperature distribution within warm-core and cold-core eddies was discussed by applying eddy advection effects. The warm water close to the equator is carried northward by the eddy's anticyclonic motion and the head of the warm-core eddy was heated up. Colder water was carried from the northern region to the head region of cold-core eddies. This explains the reversal of the horizontal temperature distribution within warm-core and cold-core eddies.

Finally, near real-time satellite altimetry was used in this study mainly on physical analysis of mesoscale eddies generated in the Northwestern region of the Hawaiian Islands. It is clear that the data sets derived from such altimeters help explain many important features of warm-core and cold-core eddies. It has emerged that eddies are really active in terms of transporting heat, trace elements, biological communities, and nutrients. Clearly eddies impact biological activity in the ocean. It is particularly difficult to examine eddy activity without fully understanding the detail of mesoscale eddies.

References

AVISO/Altimetry (1997) AVISO User Services for Sea Level Anomaly Altimeter products, CN, CLS Space Oceanography Division, Toulouse, France. (accessible from the World Wide Web server at http://www.aviso.oceanobs.com/html/portail/general/welcome_uk.php3)

Chelton, B.D. and Schlax, G.M. (1996) Global observations of oceanic Rossby waves. SCIENCE, Vol. 272, 234 – 238.

Ebuchi, N. and Hanawa, K. (2001) Trajectory of mesoscale eddies in the Kuroshio recirculation region. Journal of Oceanography, Vol. 57, pp 471 – 480

Jacobs, G.A. and et al. (2002) Operational altimeter sea level products. Oceanography, Vol. 15, No. 1, 13 – 21.

Jakobsen, K. P., (2000) Mesoscale eddies in the Nordic seas: Spatiotenporal variability and their relation to deep-sea convection investigated by use of Lagrangian surface drifters. Master thesis in Physics and Geography. Roskilde Universitecenter.

Jayne, R.S. and Marotzke (2002) The oceanic eddy heat transport. Journal of Physical Oceannography, 32, 3328-3345.

Kusakabe, M., Andreev, A., Lobanov, V., Zhabin, I., Kumamoto, Y., and Murata, A. (2002) Effects of the anticyclonic eddies on water masses, chemical parameters and chlorophyll distributions in the Oyashio current region. Journal of Oceanography, Vol. 58, pp. 691-701

Leeuwenburgh, O. and Stammer, D. (2001) The effect of ocean currents on Sea Surface Temperature Anomalies. Journal of Oceanography, Vol. 31, 2340 – 2353.

Martin, A.P. and Pondaven, P. (2003) On estimates for the vertical nitrate flux due to eddy pumping. Journal of Geophysical Research, Vol. 108, No.C11, 3359, 23-1-23-9.

Mitchum, G.T. (1995) On using satellite altimetric heights to provide a spatial context for the Hawaii Ocean Time-series measurements. Deep-Sea Research Ⅱ, Vol. 43, No 2-3, pp. 257 – 280.

Perkins, S. (2003) Oceans Aswirl: Massive eddies influence Earth's climate, marine ecosystems, even big business. Science News, Vol. 163, No. 24, p375

Qiu, B. et al. (1997) Existence and formation mechanism of the North Hawaiian Ridge Current. 27, 431-444

Qiu, B. and Chen, S. (2004) Eddy-induced heat transport in the subtropical North Pacific from Argo, TMI and altimetry measurements. Journal of Physical Oceanography, in press.

Qiu, B. and Chen, S. (2004) Seasonal modulations in the eddy field of the South Pacific Ocean. Journal of Physical Oceanography, Vol. 34, 1515 – 1527

Rhines, P.B. (2001) Mesoscale eddies. University of Washington, School of Oceanography, Academic Press.

Sakamoto, C.M and et al. (2004) Influence of Rossby waves on nutrient dynamics and the plankton community structure in the North Pacific subtropical gyre. Journal of Geophysical Research, Vol. 109, C05032, 1-12.

Seki, M.P. and et al. (2002) An oceanographic characterization of swordfish longline fishing grounds in the springtime subtropical North Pacific. Fisheries Oceanography, 11:5, 251 – 256.